High-power wavelength-swept laser in Littman telescope-less polygon filter and dual-amplifier configuration for multichannel optical coherence tomography

Michael K. K. Leung,[1] Adrian Mariampillai,[1] Beau A. Standish,[1] Kenneth K. C. Lee,[1] Nigel R. Munce,[1] I. Alex Vitkin,[1,2] and Victor X. D. Yang[3,*]

[1]*Department of Medical Biophysics, University of Toronto, Toronto, Ontario M5G 2M9, Canada*
[2]*Department of Radiation Oncology, University of Toronto, Toronto, Ontario M5G 2M9, Canada*
[3]*Department of Computer and Electrical Engineering, Ryerson University, Toronto, Ontario M5B 2K3, Canada*
[*]*Corresponding author: yangv@ee.ryerson.ca*

Received May 28, 2009; revised August 4, 2009; accepted August 5, 2009;
posted August 19, 2009 (Doc. ID 111987); published September 10, 2009

We report a high-power wavelength-swept laser source for multichannel optical coherence tomography (OCT) imaging. Wavelength tuning is performed by a compact telescope-less polygon-based filter in Littman arrangement. High output power is achieved by incorporating two serial semiconductor optical amplifiers in the laser cavity in Fourier domain mode-locked configuration. The measured wavelength tuning range of the laser is 111 nm centered at 1329 nm, coherence length of 5.5 mm, and total average output power of 131 mW at 43 kHz sweeping rate. Multichannel simultaneous OCT imaging at an equivalent A-scan rate of 258 kHz is demonstrated. © 2009 Optical Society of America

OCIS codes: 110.4500, 140.3600, 170.3880, 170.4500.

Optical coherence tomography (OCT) is an emerging noninvasive cross-sectional imaging modality that is becoming increasingly important in biomedical applications. Its advance is further driven by improvements in sensitivity and higher frame rates with the development of frequency domain acquisition techniques [1]. One implementation is swept-source OCT (SS-OCT), where the wavelength of the light source is tuned in time to allow reconstruction of depth-resolved axial scan or A-line [2]. Key source characteristics include wide tuning ranges for high spatial resolution, narrow instantaneous linewidth for large ranging depths, and sufficient output power for high sensitivity. High output power also benefits multichannel OCT (MOCT) systems, where multiple sample arms are used to image several regions at once. Major advantages of MOCT include faster image acquisition rates without a corresponding increase in the tuning speed and required bandwidth for detector and data acquisition. High-speed imaging can also reduce undesirable imaging artifacts, and is important *in vivo*, where organ motion can affect the image quality, especially when acquiring large volumetric data sets. MOCT can also potentially improve Doppler OCT (DOCT) by reducing motion artifacts while keeping the A-scan repetition rate slow enough to allow phase buildup for detection of slow-moving flow [3,4]. Finally, MOCT may be used to improve the lateral resolution by simultaneously imaging a sample with multiple beams focused at different depths [5].

Two wavelength tuning schemes have been demonstrated for SS-OCT, namely, the fiber Fabry–Perot tunable filter (FFP-TF) and the polygon mirror configuration [6,7]. The former setup uses piezoelectric-actuated FFP-TF to produce sinusoidal, bidirectional wavelength sweeps. To produce unidirectional sweeps, buffered cavity designs have been proposed [6]. In the polygon mirror configuration, diverging angularly dispersed light from a grating is focused through a telescope onto a rotating polygon mirror to generate unidirectional linear wavelength sweeps [8,9]. Although the polygon filter-based laser requires bulk optics and complex alignment, it may be more suitable for MOCT, since it can deliver higher power without the need for booster amplification at the output. Moreover, native unidirectional sweeping is beneficial for DOCT, since consecutive A-scans can be used for phase comparison.

In rotating polygon configurations, two compact designs based on using a diffraction grating in Littrow arrangement have been described [10]. With both configurations, the polygon is illuminated first, followed by the grating. Such telescope-less design leads to easier alignment, less power losses from the optics, shorter cavity length, and smaller footprint that may be beneficial for clinical use. In the first design, the diffraction grating is illuminated one time. Although the filter has a large tuning range, the instantaneous linewidth of the laser output is compromised. To decrease the linewidth, prism expanders are used to increase the beam width incident on the grating [11]. In the second design, the linewidth is narrowed by three diffractions off the grating. However, multiple facets of the polygon are required, contributing to beam clipping, reduced duty cycle, and decreased output power.

In this Letter, we describe a high output power and compact telescope-less wavelength-swept laser source based on the polygon scanning mirror for MOCT. We added an end reflector mirror to couple diffracted light from the grating back into the laser

0146-9592/09/182814-3/$15.00

cavity in Littman arrangement that improves the linewidth, compared with the single diffraction Littrow configuration, and reduces beam clipping. We also introduce a laser cavity in Fourier-domain mode-locking (FDML) configuration that combines two semiconductor optical amplifiers (SOAs) positioned serially for increased output power. The laser has a measured edge-to-edge tuning range of 111 nm centered at 1329 nm and a coherence length of 5.5 mm.

Figure 1(a) depicts the filter configuration. Wavelength tuning is performed by using the polygon mirror to scan the beam across the diffraction grating. Depending on the incident angle of the beam, a particular wavelength will be retroreflected from the end mirror back into the cavity. Assuming no beam clipping, the free spectral range (FSR) of this filter is given by

$$\mathrm{FSR} = d\Delta\theta\cos(\theta_0), \tag{1}$$

where d, $\Delta\theta$, and θ_0 are the grating pitch, sweep angle per facet, and incident angle at the center wavelength λ_o, respectively. The incident angle depends on the angle δ between the grating and the end reflector mirror by the grating equation $\theta_0 = \sin^{-1}(\lambda_o/d - \sin(\delta))$. The grating is illuminated twice for each pass through the filter. The instantaneous linewidth is reduced by a factor of 2 compared with the Littrow configuration [10]. One drawback of the Littrow design is that the beam incident angle to the grating must be fixed such that the diffracted light returns to the cavity. In the current Littman design, δ can be adjusted. This makes it possible to adjust the grating and end reflector mirror angle for θ_0 to be close to the grazing incidence to maximize efficiency, and provides some freedom to tune the filter center wavelength.

The filter was constructed using a 72-facet polygon scanner (SA34, Lincoln Laser), 1200 lines/mm blazed diffracting grating (GR50-1210, Thorlabs), and a gold mirror (ME2S-M01, Thorlabs). The polygon facet width is 2.77 mm, and the collimator has a $1/e^2$ beam width of 1.9 mm. The grating is placed ~7 cm away from the polygon, and the center-to-center distance between the mirror and grating is ~4 cm. By changing θ_0 and δ, the center wavelength of the laser can be adjusted. The chosen center wavelength was 1329 nm to trigger a fiber Bragg grating (FBG) used to prompt the beginning of each sweep sequence. Narrower linewidth can be achieved by increasing the incident entrance angle at the expense of reduced FSR and grating efficiency. For an FSR of 111 nm, the incident angle θ_0 at the center wavelength was set to 40.4°, and the angle δ between the grating and mirror was 70°. This corresponds to a sweep angle $\Delta\theta$ of 10°, or the entire scan angle of each polygon facet, according to Eq. (1). The gain medium of the laser consisted of two SOAs (BOA1017, Covega) with peak amplified spontaneous emission (ASE) wavelength at 1320 nm. Figure 1(b) shows the arrangement of the cavity, set up in a ring configuration with a fiber length of 7.8 m and a 4.8 km SMF28e fiber spool for FDML operation [8,12]. The first output taps off 70% of the power from SOA 1, so the second SOA is not saturated. At the second output, only 50% of the power from SOA 2 was coupled out to accommodate losses in the filter. Three polarization controllers were used to align the polarization states of the two SOAs and the filter.

Figure 2(a) shows the spectra of the laser outputs measured with an optical spectrum analyzer (AQ6331, Yokogawa). Besides difference in intensity, both spectra are similar in profile and are centered at 1329 nm with an edge-to-edge tuning range of 111 nm at 43 kHz scan rate. Figure 2(b) shows the power of the laser as a function of injection current, varied together at both SOAs. At 500 mA, the power at the first and second output is 72.9 mW and 58.7 mW, respectively. The point-spread functions measured with an 80 MHz balanced detector at various depths are plotted in Fig. 2(c). The reference arm power was attenuated for the measurements. The 6 dB drop in amplitude at both outputs is located at 2.75 mm, or 5.5 mm full range depth, which corresponds to a linewidth of 0.14 nm. Figure 2(d) shows the interference signal captured at 1.5 mm depth, showing minimal dead time between each wavelength sweep.

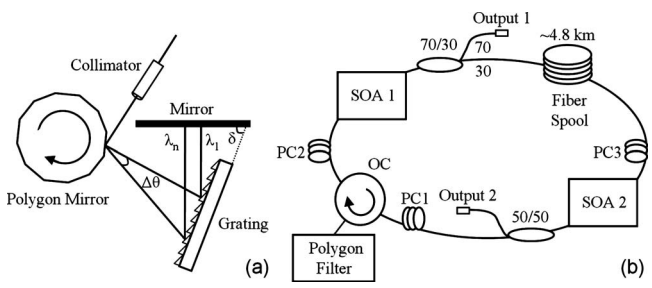

Fig. 1. (a) Schematic diagram of the polygon filter configuration. Sweep direction is in increasing wavelengths. (b) Configuration of the ring cavity laser for multichannel SS-OCT. PC, polarization controller; SOA, semiconductor optical amplifier; OC, optical circulator.

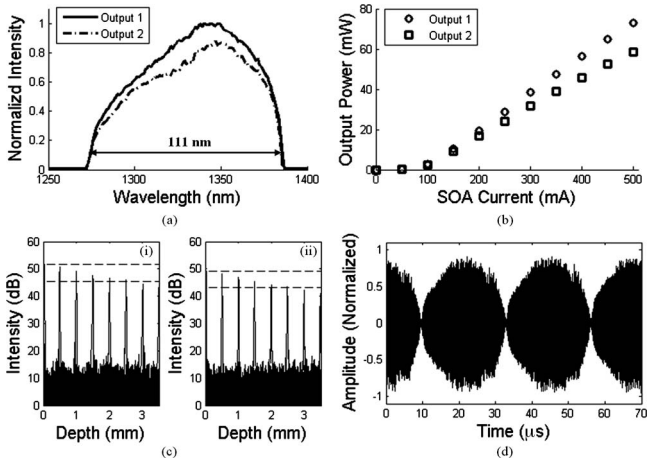

Fig. 2. (a) Spectra and (b) average output power versus injection current of the FDML laser at the first and second output. (c) Point-spread function at different depths up to 3.5 mm for laser outputs (i) one and (ii) two. The dotted lines mark the intensity at zero delay and at 6 dB drop. (d) Interference signal at a depth of 1.5 mm showing three complete tuning cycles.

The dual-SOA cavity was tested in short-cavity and FDML configurations. In the short-cavity arrangement, a full ranging depth of 4.0 mm was achieved in the first SOA, which was preceded by the polygon filter. Following the second stage of amplification, broadening of the instantaneous linewidth was observed at the second output, resulting in a reduced ranging depth of 2.8 mm. To improve the performance of both outputs for multichannel imaging, FDML was used. In this operation regime, narrow laser linewidth is preserved regardless of the photon lifetime, and a quasi-stationary state is maintained within the cavity [12]. With FDML, the overall linewidth of the laser improved, and the disparity in ranging depth at both outputs was also reduced. There were negligible differences in the measured ranging depth. Both outputs have sufficient power to drive multiple channels simultaneously, and ASE was not observed to significantly affect the imaging capabilities of the second channel.

Using this laser, MOCT was demonstrated in a prototype six-channel imaging system. The imaging arm consisted of a 12-channel 250 μm core-to-core distance fan-out cable (Pacific Interconnections LLC), with the multifiber push-on (MPO) connector end attached to the shaft of a galvanometer motor (Model 6230, Cambridge Technology, Inc.). Light propagating from the bare fiber ends of the MPO connector was directed toward an achromatic doublet (25.4 mm diameter, $f = 25$ mm), placed 50 mm away. For this feasibility study, the center six of the 12 channels were used as imaging arms, each paired with a separate reference mirror, to achieve 258 kHz effective A-scan rate. All six channels were focused at the same depth, each imaging a separate strip of the sample with edge overlap for image fusion. Each of the two outputs from the laser powered three channels. Data acquisition (DAQ) of the six imaging channels was simultaneously performed using two separate computers. A dual-core computer with a two-channel DAQ card (ATS460, AlazarTech) recorded data from two channels. The remaining four channels were acquired by a quad-core computer with a PXI chassis and two two-channel DAQ cards (NI 5122, National Instruments). Figure 3 shows an image of the human nail fold obtained with the MOCT system. Future work will involve inclusion of additional imaging channels, optimization of the multichannel sample arm optics to equalize sensitivity, and Doppler imaging.

In summary, a high-power wavelength-swept laser based on a compact telescope-less polygon filter and two serial SOAs was demonstrated. A six-channel OCT system was constructed to show the feasibility of the laser for MOCT imaging with increased effective A-scan rate, which may benefit three-dimensional *in vivo* imaging where bulk tissue motion can adversely affect the image quality.

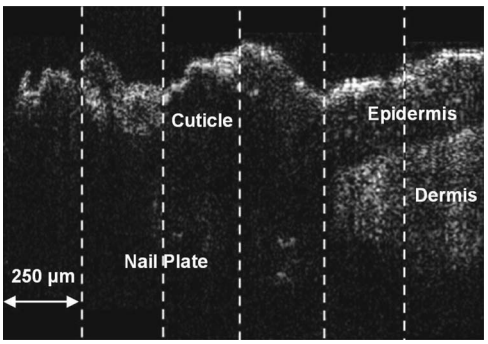

Fig. 3. Structural image of the human nail fold acquired using the MOCT system. The image depth is 1.5 mm. Each channel spans a distance of 250 μm and is separated by a dotted line.

This research was supported by the Natural Science and Engineering Research Council of Canada, the Canadian Foundation for Innovation, and the Canadian Institutes of Health Research. The authors acknowledge James Jiang (Thorlabs) for valuable technical support during this experiment.

References

1. M. A. Choma, M. V. Sarunic, C. Yang, and J. A. Izatt, Opt. Express **11**, 2183 (2003).
2. S. H. Yun, G. J. Tearney, J. F. De Boer, N. Iftimia, and B. E. Bouma, Opt. Express **11**, 2953 (2003).
3. V. X. D. Yang, M. L. Gordon, B. Qi, J. Pekar, S. Lo, E. Seng-Yue, A. Mok, B. C. Wilson, and I. A. Vitkin, Opt. Express **11**, 794 (2003).
4. S. Makita, M. Yamanari, and Y. Yasuno, Proc. SPIE **7372**, 73721M (2009).
5. V. X. D. Yang, N. Munce, J. Pekar, M. L. Gordon, S. Lo, N. E. Marcon, B. C. Wilson, and I. A. Vitkin, Opt. Lett. **29**, 1754 (2004).
6. R. Huber, D. C. Adler, and J. G. Fujimoto, Opt. Lett. **31**, 2975 (2006).
7. W. Y. Oh, S. H. Yun, G. J. Tearney, and B. E. Bouma, Opt. Lett. **30**, 3159 (2005).
8. G. Y. Liu, A. Mariampillai, B. A. Standish, N. R. Munce, X. Gu, and I. A. Vitkin, Opt. Express **16**, 14095 (2008).
9. S. H. Yun, C. Boudoux, G. J. Tearney, and B. E. Bouma, Opt. Lett. **28**, 1981 (2003).
10. S. M. R. Motaghian Nezam, Opt. Lett. **33**, 1741 (2008).
11. C. Chong, A. Morosawa, and T. Sakai, IEEE J. Sel. Top. Quantum Electron. **14**, 235 (2008).
12. R. Huber, M. Wojtkowski, and J. G. Fujimoto, Opt. Express **14**, 3225 (2006).